Nonthermal Bonding Origin of a Novel Photoexcited Lattice Instability in SnSe

Yijing Huang,[1,2,3,4,*] Samuel Teitelbaum,[2,4,5] Shan Yang,[6] Gilberto De la Peña,[2,4] Takahiro Sato,[7] Matthieu Chollet,[7] Diling Zhu,[7] Jennifer L. Niedziela,[6,8] Dipanshu Bansal,[6,9] Andrew F. May,[8] Aaron M. Lindenberg,[2,4,10] Olivier Delaire,[6,11,12] Mariano Trigo,[2,4] and David A. Reis[2,3,4,13,†]

[1]*Department of Physics, University of Illinois at Urbana-Champaign, Urbana, Illinois 61801, USA*
[2]*Stanford Institute for Materials and Energy Sciences, SLAC National Accelerator Laboratory, Menlo Park, California 94025, USA*
[3]*Department of Applied Physics, Stanford University, Stanford, California 94305, USA*
[4]*Stanford PULSE Institute, SLAC National Accelerator Laboratory, Menlo Park, California 94025, USA*
[5]*Department of Physics, Arizona State University, Tempe, Arizona 85287, USA*
[6]*Department of Mechanical Engineering and Materials Science, Duke University, Durham, North Carolina 27708, USA*
[7]*Linac Coherent Light Source, SLAC National Accelerator Laboratory, Menlo Park, California 94025, USA*
[8]*Materials Science and Technology Division, Oak Ridge National Laboratory, Oak Ridge, Tennessee 37831, USA*
[9]*Department of Mechanical Engineering, Indian Institute of Technology Bombay, Mumbai, Maharashtra 400076, India*
[10]*Department of Materials Science and Engineering, Stanford University, Stanford, California 94305, USA*
[11]*Department of Physics, Duke University, Durham, North Carolina 27708, USA*
[12]*Department of Chemistry, Duke University, Durham, North Carolina 27708, USA*
[13]*Department of Photon Science, Stanford University, Stanford, California 94305, USA*

(Received 21 February 2023; accepted 6 September 2023; published 12 October 2023)

Lattice dynamics measurements are often crucial tools for understanding how materials transform between different structures. We report time-resolved x-ray scattering-based measurements of the nonequilibrium lattice dynamics in SnSe, a monochalcogenide reported to host a novel photoinduced lattice instability. By fitting interatomic force models to the fluence dependent excited-state dispersion, we determine the nonthermal origin of the lattice instability to be dominated by changes of interatomic interactions along a bilayer-connecting bond, rather than of an intralayer bonding network that is of primary importance to the lattice instability in thermal equilibrium.

DOI: 10.1103/PhysRevLett.131.156902

The interatomic forces that determine materials' structure and dynamics can be modified by temperature, pressure, chemical composition, and applied fields, leading to new equilibrium phases with dramatically different electronic, thermal, and mechanical properties [1–3]. Inelastic scattering measurements using x-ray [4–6] or neutron [7,8] can reveal microscopic details of interatomic interactions that lead to phase transitions. We extend such an idea to femtosecond x-ray diffuse scattering, by measuring temporal coherences in the mean-square atomic displacements associated with a rapid change in the interatomic forces, as a function of momentum transfer [9–12]. The method allows access to phonon dispersions on short timescales, and hence allows extraction of interatomic interactions involved in the generation of nonequilibrium states, which may possess properties that do not exist in the equilibrium [13].

Here we report nonequlibrium lattice dynamics study of the monochalchogenide SnSe, which we recently demonstrated hosts a novel lattice instability upon photoexcitation using ultrafast x-ray diffraction [14]. As diffraction yields information on the average structure and dynamics within the unit cell, it can tell us about changes in bond lengths. However, ultimately time- and momentum-resolved lattice dynamics measurements such as reported here are required to access the collective excitations over a range of length scales which gives information on how and which interatomic forces change upon photoexcitation. By fitting interatomic force models to the fluence-dependent excited-state dispersion, we demonstrate the nonthermal nature of the interatomic bonding in the photoexcited state of SnSe. The changes of interatomic interactions along an interlayer bond lead to the photoexcited-state lattice instability in Ref. [14], which is distinct from the well-known high-temperature phase. In contrast, the lattice instability in thermal equilibrium is associated with the intralayer bonding network.

In some of the IV–VI, V, V_2VI_3 semiconductors, a valence-unsaturated p orbital bonding network is formed due to the large energy separation in the s and p orbitals [15] and is known to give rise to important properties including low thermoconductivity, instability of the lattice [16], large polarizability [17], and large change of optical constants upon phase change [18]. These correspond to applications including thermoelectric, ferroelectric, and phase change materials. Such a valence-unsaturated p

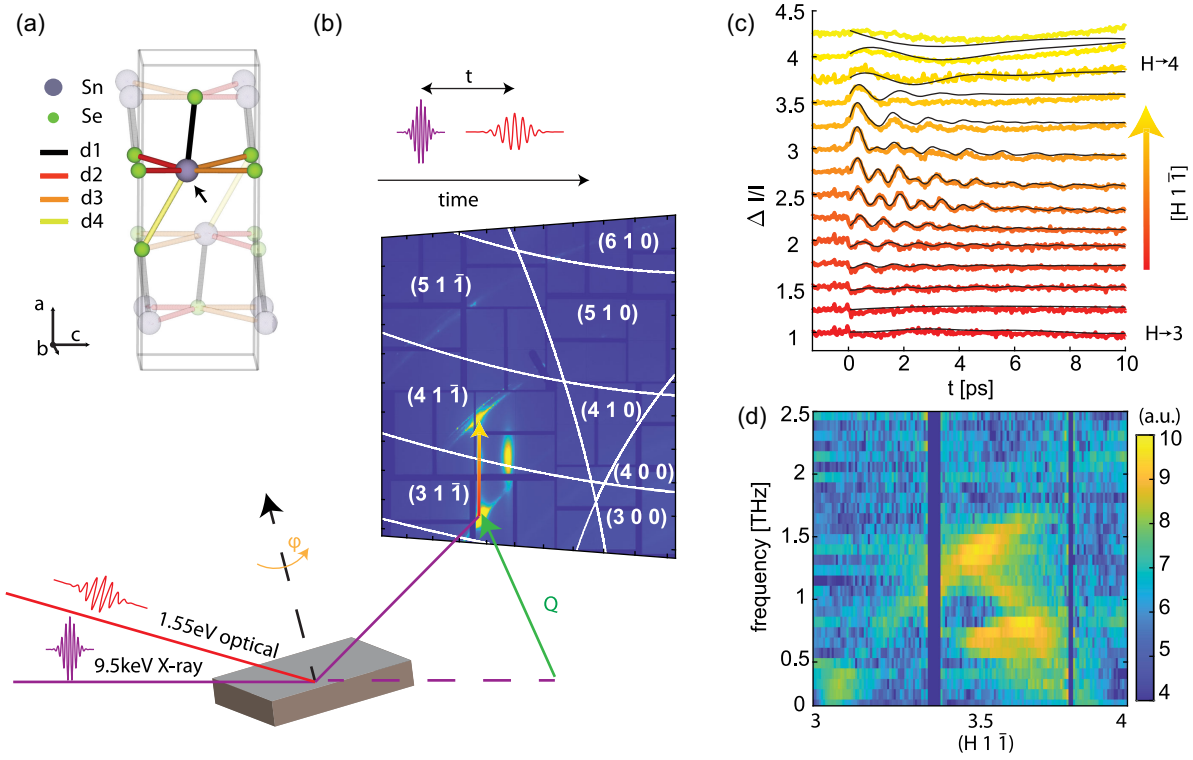

FIG. 1. (a) The unit cell of the *Pnma* phase of SnSe illustrates the d_1-d_4 bonds derived from nearest neighbor bonds in the parent cubic structure. (b) The experimental setup. The sample can be rotated around its normal by an azimuthal angle φ, and a 2D detector captures the diffuse scattering intensity as a function of delay t between the optical pump and x-ray probe. The green vector shows the momentum transfer **Q**, associated with scattering on a particular pixel on the detector. The detector image shows the typical intensity pattern for a fixed φ. White lines represent the Brillouin zone boundaries of the *Pnma* structure. (c) Time dependence of the relative intensity for representative **Q** along $(H1\bar{1})$, $H \in [3, 4]$. Black lines show LPs. (d) The magnitude of the Fourier transform of time traces as those shown in Fig. 1(c).

orbital bonding network has been dubbed "resonant bonding" [11,16,18–20] in analogy with the concept from Pauling's work on benzene [21]. In this case, the p orbital (p_x, p_y, p_z) bonding network naturally leads to three orthogonal atomic chains [22,23] and thus a rocksaltlike structure as the parent structure. The key properties of the p orbital bonding network originate from its long-range interactions along one or more of the three chains [11,16,19,23]. Wuttig *et al.* [24] note that the properties are fundamentally different from resonant bonding in benzene and graphene, and that the long-range p orbital bonding features bonding characteristics distinct from metallic, ionic, or covalent bonds, leading them to describe the bonding as "metavalent" [25,26].

SnSe, as material from this group, is of orthorhombic space group *Pnma* at room temperature. The structure is a distortion from the rocksaltlike parent structure and features a stacking of bilayers along the **a** axis. The valence-unsaturated p orbital bonding network lies in the **b**-**c** (y-z) plane. Frozen phonon calculations show that in the equilibrium, soft phonon displacement induces long-range charge-density perturbations along p bonding directions in the **b**-**c** plane [27], i.e., the p orbital bonding direction, which explains the soft phonon that leads to the thermal phase transition to the *Cmcm* structure, as well as the large anharmonicity that leads to low thermoconductivity [27,28]. Raman measurements show that the Raman-active modes which experience significant frequency softening upon the thermal *Pnma-Cmcm* transition are those polarized in the **b**-**c** plane along **c** rather than those along **a** [29,30]. Thus, it is confirmed in SnSe that in thermal equilibrium, lattice instability and the large anharmonicity originated from the unsaturated p network with long-range interatomic interactions. We show in Fig. 1(a) the six nearest neighbor bonds of the rocksalt structure that become four inequivalent bonds in *Pnma*. In particular, the d_2 and d_3 bonds primarily along [011] and $[01\bar{1}]$ directions belong to the unsaturated p orbital bonding network, the bilayer-connecting d_4 bond is largely tilted from the octahedral coordination of a parent structure. Based on density function theory (DFT) calculation of interatomic forces, d_4 is a much weaker bond than d_1, and thus does not belong to part of the p-orbital bonding network with long-range interactions. However, by fitting an interatomic force model to the excited state phonon dispersions, we found that it is the change in interatomic

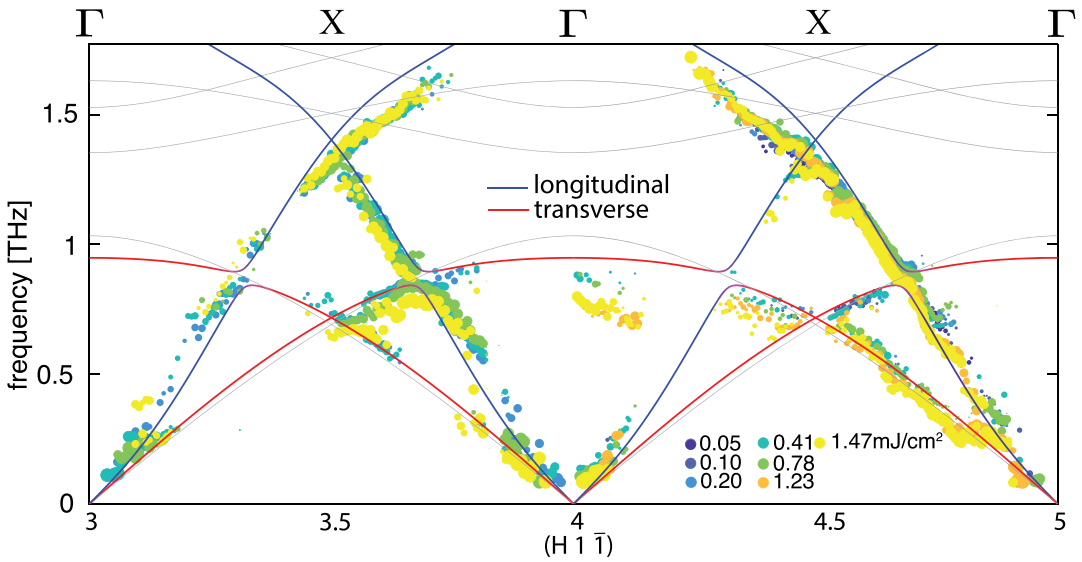

FIG. 2. Low-frequency phonons of photoexcited SnSe propagated along the a direction ($\mathbf{Q} = (H1\bar{1})$, $H \in [3,5]$), extracted from LPs. The solid lines are the ground state phonon dispersion based on DFT. Red and blue lines represent $T(\mathbf{c})$ and $L(\mathbf{a})$, respectively.

interaction of the bilayer-connecting d_4 bond, rather than the in-plane bonds, that destabilizes the SnSe structure and leads to soft phonons in its photoexcited state.

The experiment was performed at the x-ray pump-probe (XPP) end station at the Linac Coherent Light Source (LCLS) free electron laser using 9.5 keV x rays [10,31]. The 1.55 eV near-infrared (NIR) pump pulses were derived from a Ti:sapphire laser. We show the experimental setup in Fig. 1(b). The x rays illuminated the sample at a fixed grazing incidence to approximately match the penetration depth with the (p polarized) NIR laser. The Cornell-SLAC pixel array detector [32] is placed ~100 mm behind the sample, which allows us to map out a large portion of the Ewald sphere when rotating the sample about the sample surface normal (azimuth φ).

In Fig. 1(c) we show diffuse scattering intensity as a function of the pump-probe delay t, for selected scattering vectors or momentum transfer, $\mathbf{Q} = (H1\bar{1})$ where $H \in [3,4]$ in reciprocal lattice units of the orthorhombic $Pnma$ structure. Figure 1(d) shows the magnitude of the Fourier transform of time-domain data, clearly displaying dispersive modes. We extract the oscillator parameters by linear prediction (LP) assuming that the data is composed of decaying cosines [33–35]. The LP is shown with black lines in Fig. 1(c) which reproduce the data well.

Figure 2 shows the photoexcited phonon dispersion and combines data collected over $\mathbf{Q} = (H1\bar{1})$, ($H \in [3,5]$). The size of the dots represents the log-scaled LP amplitude of the oscillations, while the colors of the dots represent different pump fluences. The solid lines show the phonon dispersion computed from DFT. The branches shown in red are the **c**-polarized transverse acoustic (TA) branch which folds into the lowest transverse optical (TO) branch [TO and TA are referred to as $T(\mathbf{c})$]. Similarly, the blue line shows the **a**-polarized longitudinal acoustic (LA) branch that folds into the lowest longitudinal optical (LO) branch [referred to together as $L(\mathbf{a})$]. The assignment of $L(\mathbf{a})$ and $T(\mathbf{c})$ phonon branches with reduced wave vectors $\mathbf{q} = (h00)$ [along $\mathbf{\Gamma}(h=0) - \mathbf{X}(h=0.5)$] is based on the phonon polarization selectivity of the phonon structure factor. **b**-polarized modes are not observed.

We show in Figs. 3(a) and 3(b) the measured fluence dependence of the $T(\mathbf{c})$ and $L(\mathbf{a})$ mode frequencies for multiple H values. The entire $T(\mathbf{c})$ branches soften with fluence, most significantly at the folded zone center ($H = 4$), and resembles the softening with temperature across the $Pnma$-$Cmcm$ transition (see Supplemental Material [36], Fig. 3). However, the frequency of $L(\mathbf{a})$ is nonmonotonic with fluence, most pronounced near the avoided crossing in Fig. 2. In order to gain insight into interatomic interactions that are responsible for the photoexcited lattice dynamics reflected in changes of phonon frequencies, we fit an interatomic force model to the measured dispersion. We define entries of the pairwise interatomic force tensor between two atoms connected by bond d_n as $F_n(i,j)$ [45]. We perform least-square fitting to measured $T(\mathbf{c})$ and $L(\mathbf{a})$ frequencies by adjusting a subset of the $F_n(i,j)$. The long-range interatomic pairs from the p bonding network are incorporated, and we assume no knowledge of the atomic position change upon photoexcitation (see Supplemental Material [36], Sec. I).

The fitting results and the correlation analysis suggest that, under photoexcitation, the bilayer-connecting d_4 bond is more responsible for phonon softening and lattice instability compared to in-plane bonds along [011] and [01$\bar{1}$]. We find that the modification to a single force constant $F_4(x,x)$ dominates the observed changes in $L(\mathbf{a})$ frequencies, and similarly $F_4(z,z)$ for $T(\mathbf{c})$. Figure 3(c)

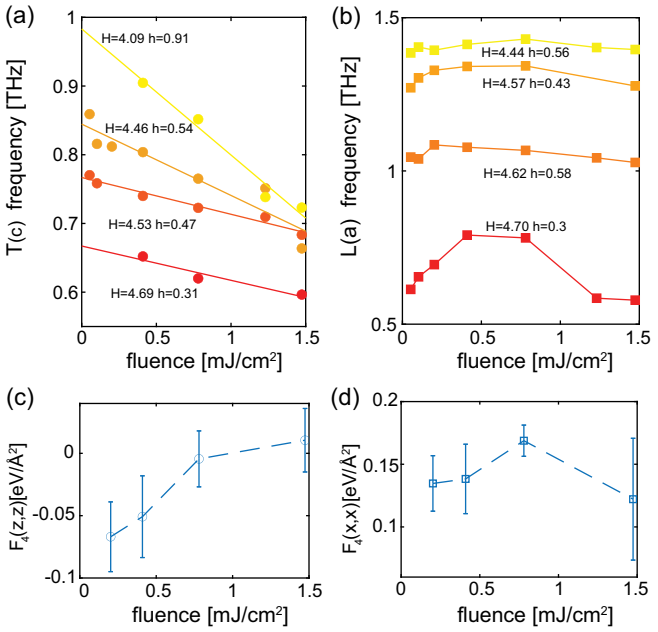

FIG. 3. (a) Near linear fluence dependent softening of $T(\mathbf{c})$ phonon in photoexcited SnSe along $(\mathrm{H}1\bar{1})$, $H \in [4,5]$ for a subset of $\mathbf{Q}$ points. (b) Nonmonotonic fluence dependence of $L(\mathbf{a})$ phonon along $(H1\bar{1})$, $H \in [4,5]$ for a subset of $\mathbf{Q}$ points. (c) The $F_4(z,z)$ forces as fitted from the experimental data. The four data points are an average of fitting results to datasets taken under different $(H1\bar{1})$, $H \in [3,4]$, and $H \in [4,5]$, and the same fluences. The error bars reflect the standard deviation of these fitting results. (d) The $F_4(x,x)$ forces as fitted from the experimental data.

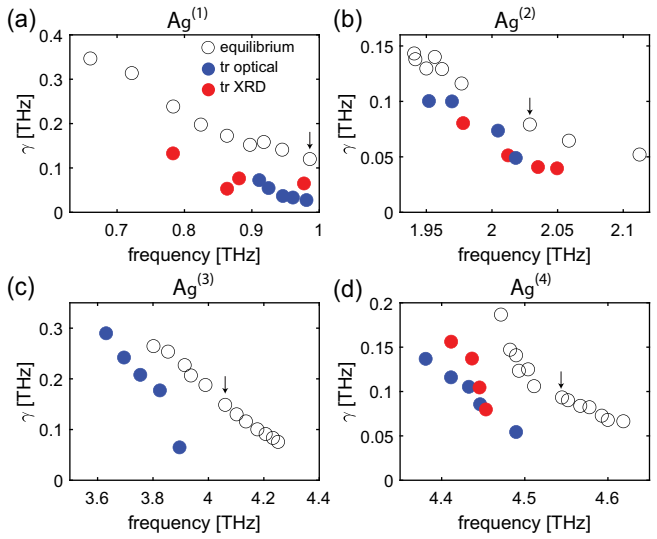

FIG. 4. Damping constants, γ, of A_g Raman modes in SnSe [(a) $(A_g^{(1)})$, (b) $(A_g^{(2)})$, (c) $(A_g^{(3)})$, (d) $(A_g^{(4)})$]. Phonon linewidths of photoexcited states (red dots, time-resolved x-ray scattering, blue dots, time-resolved optical reflectivity) are consistently lower than the thermal equilibrium (black circle, Raman scattering from Refs. [29,30,56]) at the same given phonon frequencies. Black arrows correspond to room temperature Raman measurements.

[Fig. 3(d)] shows the average value of $F_4(z,z)$ $[F_4(x,x)]$ independently fitted to the two datasets $H \in [3,4]$ and $H \in [4,5]$ in Fig. 2. Figure 3(c) suggests an increase of the negative $F_4(z,z)$ upon increased fluence, which is well correlated to the monotonic $T(\mathbf{c})$ softening under photoexcitation. The fluence dependence of fitting results $F_4(x,x)$ as shown in Fig. 3(d), is well correlated to the nonmonotonic $L(\mathbf{a})$ fluence dependence behavior under photoexcitation [46]. Even as long-range in-plane bonds along [011] and $[01\bar{1}]$ are included in the fitting model, the fitted force tensors for these bonds do not correlate significantly with the mode softening. This attests to a nonthermal bonding origin for the lattice instability in photoexcited SnSe.

Consistent with the nonthermal nature of the interatomic bonding, we show below that the photoexcited lattice is more harmonic than the thermal one at the temperature that produces a similar level of softening of the symmetric Raman active A_g modes at the zone center. We compare the phonon damping rate γ [50] versus the frequency, as the latter maps to phonon softening, which can be taken as a measure of the proximity to a phase transition [51]. In Figs. 4(a)–4(d) we show γ for all four A_g modes observed under photoexcitation and in equilibrium. Even as intraband phonon scattering [52–55] significantly contributes to an increased phonon linewidth in the photoexcited states, the phonon damping rate under photoexcitation is consistently lower than its counterpart under thermal equilibrium. The data indicate that the photoexcited lattice is much more harmonic than the lattice at a similar proximity to the thermal phase transition. Such observations have to do with the fact that the anharmonicity of a solid in thermal equilibrium is developed through a significant change in the lattice constants and internal atomic coordinates, which do not happen under photoexcitation on a short timescale. We conclude that the lattice instability under photoexcitation does not originate from the p orbital bonding as in thermal equilibrium, but rather, the weakened interbilayer coupling which suppresses the frequency of the $T(\mathbf{c})$ propagated along $(h00)$, and destabilizes the structure. Density functional theory based calculations in Ref. [27] suggest a relatively high electronic density of the Sn $5s$-Se $4p_x$ orbital localized near the area pointed by the black arrow in Fig. 1(a), close to d_4. We infer that it is the depopulation of these orbitals that leads to the relatively significant change in the interatomic interaction of d_4 bond. This is also supported by diffraction results in Ref. [14], where the d_4 is shown to experience a larger bond angle change compared to other bonds.

We provide the first example where time-resolved diffuse scattering investigates both the long-range and near-neighbor interatomic interactions and helps associate the interatomic force change with a photoinduced novel phenomenon. The result may hold implications for the excited

states in ferroelectrics and phase change materials, where the electron redistribution significantly impacts the lattice dynamics, and the structural change may couple to bonding type change. We point out that time-resolved x-ray scattering can provide insight into renormalized effective interactions in light-engineered materials or materials whose order gets quenched by light [13,57]. We suggest that time-resolved x-ray scattering which measures both atomic positions and lattice dynamics upon short-pulse excitation, can reveal the interplay between electron distribution and interatomic bonding, as well as their cooperative effects on lattice structure, paving the way to controlling materials properties under nonequilibrium conditions.

Preliminary x-ray characterization was performed at beamline 7-2 at the Stanford Synchrotron Radiation Lightsource (SSRL). Y. H., S. T., G. d. P, D. A. R., A. M. L., and M. T. were supported by the U.S. Department of Energy, Office of Science, Office of Basic Energy Sciences through the Division of Materials Sciences and Engineering under Contract No. DE-AC02-76SF00515. S. Y. acknowledges support from the Fitzpatrick Institute for Photonics through a Chambers Scholarship. O. D. acknowledges support from the U.S. Department of Energy, Office of Science, Basic Energy Sciences, Materials Sciences and Engineering Division, under Award No. DE-SC0019978. Use of the LCLS and S. S. R. L. is supported by the US Department of Energy, Office of Science, Office of Basic Energy Sciences under Contract No. DE-AC02-76SF00515. Sample synthesis and characterization (A. F. M.) was supported by the U.S. Department of Energy, Office of Science, Basic Energy Sciences, Materials Sciences, and Engineering Division. D. A. R. acknowledges discussions with Ivana Savic and Stephen Fahy. Y. H. acknowledges discussions with Xing He.

*huangyj@illinois.edu
†dreis@stanford.edu

[1] M. Born and K. Huang, *Dynamical Theory of Crystal Lattices* (Oxford University Press, 1998).
[2] E. G. Brovnman and Y. Kagan, The phonon spectrum of metals, Sov. Phys. JETP **25**, 104 (1967).
[3] L. J. Sham, Electronic contribution to lattice dynamics in insulating crystals, Phys. Rev. **188**, 1431 (1969).
[4] M. Krisch and F. Sette, Inelastic x-ray scattering from phonons, in *Light Scattering in Solid IX*, edited by M. Cardona and R. Merlin (Springer Berlin Heidelberg, Berlin, Heidelberg, 2007), pp. 317–370.
[5] A. Q. R. Baron, High-resolution inelastic x-ray scattering II: Scattering theory, harmonic phonons, and calculations, in *Synchrotron Light Sources and Free-Electron Lasers: Accelerator Physics, Instrumentation and Science Applications*, edited by E. Jaeschke, S. Khan, J. R. Schneider, and J. B. Hastings (Springer International Publishing, Cham, 2014), pp. 1–32, 10.1007/978-3-319-04507-8_52-1.
[6] A. Q. R. Baron, High-resolution inelastic x-ray scattering I: Context, spectrometers, samples, and superconductors, in *Synchrotron Light Sources and Free-Electron Lasers: Accelerator Physics, Instrumentation and Science Applications*, edited by E. Jaeschke, S. Khan, J. R. Schneider, and J. B. Hastings (Springer International Publishing, Cham, 2014) pp. 1–68, 10.1007/978-3-319-04507-8_41-1.
[7] B. N. Brockhouse and A. T. Stewart, Scattering of neutrons by phonons in an aluminum single crystal, Phys. Rev. **100**, 756 (1955).
[8] R. A. Cowley, Lattice dynamics and phase transitions of strontium titanate, Phys. Rev. **134**, A981 (1964).
[9] M. Trigo *et al.*, Fourier-transform inelastic x-ray scattering from time- and momentum-dependent phonon–phonon correlations, Nat. Phys. **9**, 790 (2013).
[10] D. Zhu, A. Robert, T. Henighan, H. T. Lemke, M. Chollet, J. M. Glownia, D. A. Reis, and M. Trigo, Phonon spectroscopy with sub-mev resolution by femtosecond x-ray diffuse scattering, Phys. Rev. B **92**, 054303 (2015).
[11] M. P. Jiang *et al.*, The origin of incipient ferroelectricity in lead telluride, Nat. Commun. **7**, 12291 (2016).
[12] S. W. Teitelbaum, T. C. Henighan, H. Liu, M. P. Jiang, D. Zhu, M. Chollet, T. Sato, E. D. Murray, S. Fahy, S. O'Mahony, T. P. Bailey, C. Uher, M. Trigo, and D. A. Reis, Measurements of nonequilibrium interatomic forces using time-domain x-ray scattering, Phys. Rev. B **103**, L180101 (2021).
[13] D. Basov, R. Averitt, and D. Hsieh, Towards properties on demand in quantum materials, Nat. Mater. **16**, 1077 (2017).
[14] Y. Huang, S. Yang, S. Teitelbaum, G. De la Peña, T. Sato, M. Chollet, D. Zhu, J. L. Niedziela, D. Bansal, A. F. May, A. M. Lindenberg, O. Delaire, D. A. Reis, and M. Trigo, Observation of a Novel Lattice Instability in Ultrafast Photoexcited SnSe, Phys. Rev. X **12**, 011029 (2022).
[15] K. Behnia, Finding merit in dividing neighbors, Science **351**, 124 (2016).
[16] S. Lee, K. Esfarjani, T. Luo, J. Zhou, Z. Tian, and G. Chen, Resonant bonding leads to low lattice thermal conductivity, Nat. Commun. **5**, 3525 (2014).
[17] K. Chang, F. Kuester, B. J. Miller, J.-R. Ji, J.-L. Zhang, P. Sessi, S. Barraza-Lopez, and S. S. Parkin, Microscopic manipulation of ferroelectric domains in snse monolayers at room temperature, Nano Lett. **20**, 6590 (2020).
[18] D. Lencer, M. Salinga, B. Grabowski, T. Hickel, J. Neugebauer, and M. Wuttig, A map for phase-change materials, Nat. Mater. **7**, 972 (2008).
[19] K. Shportko, S. Kremers, M. Woda, D. Lencer, J. Robertson, and M. Wuttig, Resonant bonding in crystalline phase-change materials, Nat. Mater. **7**, 653 (2008).
[20] J. J. Li, J. Chen, D. A. Reis, S. Fahy, and R. Merlin, Optical Probing of Ultrafast Electronic Decay in Bi and Sb with Slow Phonons, Phys. Rev. Lett. **110**, 047401 (2013).
[21] L. Pauling, *The Nature of the Chemical Bond* (Cornell University Press, Ithaca, New York, 1960).
[22] P. Littlewood and V. Heine, The infrared effective charge in IV-VI compounds. I. A simple one-dimensional model, J. Phys. C **12**, 4431 (1979).
[23] P. Littlewood, The dielectric constant of cubic IV-VI compounds, J. Phys. C **12**, 4459 (1979).
[24] M. Wuttig, V. L. Deringer, X. Gonze, C. Bichara, and J.-Y. Raty, Incipient metals: Functional materials with a unique bonding mechanism, Adv. Mater. **30**, 1803777 (2018).

[25] L. Guarneri, S. Jakobs, A. von Hoegen, S. Maier, M. Xu, M. Zhu, S. Wahl, C. Teichrib, Y. Zhou, O. Cojocaru-Mirédin, M. Raghuwanshi, C.-F. Schön, M. Drögeler, C. Stampfer, R. P. S. M. Lobo, A. Piarristeguy, A. Pradel, J.-Y. Raty, and M. Wuttig, Metavalent bonding in crystalline solids: How does it collapse?, Adv. Mater. **33**, 2102356 (2021).

[26] D. Sarkar, S. Roychowdhury, R. Arora, T. Ghosh, A. Vasdev, B. Joseph, G. Sheet, U. V. Waghmare, and K. Biswas, Metavalent bonding in gese leads to high thermoelectric performance, Angew. Chem., Int. Ed. **60**, 10350 (2021).

[27] C. W. Li, J. Hong, A. F. May, D. Bansal, S. Chi, T. Hong, G. Ehlers, and O. Delaire, Orbitally driven giant phonon anharmonicity in SnSe, Nat. Phys. **11**, 1063 (2015).

[28] T. Chattopadhyay, J. Pannetier, and H. Von Schnering, Neutron diffraction study of the structural phase transition in SnS and SnSe, J. Phys. Chem. Solids **47**, 879 (1986).

[29] T. Lanigan-Atkins, S. Yang, J. L. Niedziela, D. Bansal, A. F. May, A. A. Puretzky, J. Y. Lin, D. M. Pajerowski, T. Hong, S. Chi, G. Ehlers, and O. Delaire, Extended anharmonic collapse of phonon dispersions in SnS and SnSe, Nat. Commun. **11**, 1 (2020).

[30] F. Liu, P. Parajuli, R. Rao, P. C. Wei, A. Karunarathne, S. Bhattacharya, R. Podila, J. He, B. Maruyama, G. Priyadarshan, J. R. Gladden, Y. Y. Chen, and A. M. Rao, Phonon anharmonicity in single-crystalline SnSe, Phys. Rev. B **98**, 224309 (2018).

[31] M. Chollet, R. Alonso-Mori, M. Cammarata, D. Damiani, J. Defever, J. T. Delor, Y. Feng, J. M. Glownia, J. B. Langton, S. Nelson *et al.*, The x-ray pump–probe instrument at the linac coherent light source, J. Synchrotron Radiat. **22**, 503 (2015).

[32] S. Herrmann *et al.*, CSPAD-140k: A versatile detector for LCLS experiments, Nucl. Instrum. Methods Phys. Res. **718**, 550 (2013).

[33] H. Barkhuijsen, R. de Beer, W. Bovée, and D. van Ormondt, Retrieval of frequencies, amplitudes, damping factors, and phases from time-domain signals using a linear least-squares procedure, J. Magn. Reson. **61**, 465 (1985).

[34] B. P. Epps and E. M. Krivitzky, Singular value decomposition of noisy data: Noise filtering, Exp. Fluids **60**, 1 (2019).

[35] B. P. Epps and E. M. Krivitzky, Singular value decomposition of noisy data: Mode corruption, Exp. Fluids **60**, 1 (2019).

[36] See Supplemental Material at http://link.aps.org/supplemental/10.1103/PhysRevLett.131.156902 for the detail of data analysis and DFT calculations, which includes additional Refs. [37–44].

[37] P. E. Blöchl, Projector augmented-wave method, Phys. Rev. B **50**, 17953 (1994).

[38] G. Kresse and D. Joubert, From ultrasoft pseudopotentials to the projector augmented-wave method, Phys. Rev. B **59**, 1758 (1999).

[39] D. Bansal, J. Hong, C. W. Li, A. F. May, W. Porter, M. Y. Hu, D. L. Abernathy, and O. Delaire, Phonon anharmonicity and negative thermal expansion in SnSe, Phys. Rev. B **94**, 054307 (2016).

[40] H. Wiedemeier and F. J. Csillag, The thermal expansion and high temperature transformation of SnS and SnSe, Zeitschrift für Kristallographie—Crystalline Materials **149**, 17 (1979).

[41] M. Sist, J. Zhang, and B. Brummerstedt Iversen, Crystal structure and phase transition of thermoelectric SnSe, Acta Crystallogr. Sect. D **72**, s310 (2016).

[42] C. W. Li, J. Hong, A. F. May, D. Bansal, S. Chi, T. Hong, G. Ehlers, and O. Delaire, Orbitally driven giant phonon anharmonicity in SnSe, Nat. Phys. **11**, 1063 (2015).

[43] T. Chatterji, U. D. Wdowik, G. Jagło, S. Rols, and F. R. Wagner, Soft-phonon dynamics of the thermoelectric β-SnSe at high temperatures, Phys. Lett. A **382**, 1937 (2018).

[44] G. Kresse and J. Furthmüller, Efficient iterative schemes for *ab initio* total-energy calculations using a plane-wave basis set, Phys. Rev. B **54**, 11169 (1996).

[45] Force change on one atom in the ith direction in response to a unit displacement of the other in jth direction $(i, j \in x, y, z)$.

[46] The nonmonotonic fluence dependence of $F_4(x, x)$ is attributed to the relaxation dynamics of the photoexcited carriers, which are known to suffer from bottleneck effects in other semiconductors [47–49].

[47] R. F. Leheny, J. Shah, R. L. Fork, C. V. Shank, and A. Migus, Dynamics of hot carrier cooling in photoexcited GaAs, Solid State Commun. **31**, 809 (1979).

[48] H. M. van Driel, Influence of hot phonons on energy relaxation of high-density carriers in germanium, Phys. Rev. B **19**, 5928 (1979).

[49] E. J. Yoffa, Screening of hot-carrier relaxation in highly photoexcited semiconductors, Phys. Rev. B **23**, 1909 (1981).

[50] A damped harmonic oscillator with a trajectory $Ae^{-\gamma t}\cos(\omega_0 t + \phi)$ in the time domain will have the imaginary part of response function $\mathrm{Im}\chi(\omega) = \{2\omega\gamma/[(\omega_0^2 - \omega^2)^2 + 4\gamma^2\omega^2]\}$ on the frequency domain, which can be measured by the Raman spectroscopy.

[51] M. T. Dove, Theory of displacive phase transitions in minerals, Am. Mineral. **82**, 213 (1997).

[52] T. A. Fjeldly, F. Cerdeira, and M. Cardona, Effects of free carriers on zone-center vibrational modes in heavily doped p-type Si. I. Acoustical modes, Phys. Rev. B **8**, 4723 (1973).

[53] D. Olego and M. Cardona, Self-energy effects of the optical phonons of heavily doped p-GaAs and p-Ge, Phys. Rev. B **23**, 6592 (1981).

[54] M. L. Ledgerwood and H. M. van Driel, Picosecond phonon dynamics and self-energy effects in highly photoexcited germanium, Phys. Rev. B **54**, 4926 (1996).

[55] K. T. Tsen, J. G. Kiang, D. K. Ferry, and H. Morkoç, Subpicosecond time-resolved Raman studies of LO phonons in GaN: Dependence on photoexcited carrier density, Appl. Phys. Lett. **89**, 112111 (2006).

[56] P. Wu, F.-R. Fan, M. Hagihala, M. Kofu, K. Peng, Y. Ishikawa, S. Lee, T. Honda, M. Yonemura, K. Ikeda, T. Otomo, G. Wang, K. Nakajima, Z. Sun, and T. Kamiyama, Strong lattice anharmonicity exhibited by the high-energy optical phonons in thermoelectric material, New J. Phys. **22**, 083083 (2020).

[57] A. de la Torre, D. M. Kennes, M. Claassen, S. Gerber, J. W. McIver, and M. A. Sentef, Colloquium: Nonthermal pathways to ultrafast control in quantum materials, Rev. Mod. Phys. **93**, 041002 (2021).